CrossMark

ORIGINAL PAPER

The influence and biomechanical role of cartilage split line pattern on tibiofemoral cartilage stress distribution during the stance phase of gait

Vickie B. Shim[1,2] · Thor F. Besier[1,3] · David G. Lloyd[2,4] · Kumar Mithraratne[1] · Justin F. Fernandez[1,3]

Abstract This study presents an evaluation of the role that cartilage fibre 'split line' orientation plays in informing femoral cartilage stress patterns. A two-stage model is presented consisting of a whole knee joint coupled to a tissue-level cartilage model for computational efficiency. The whole joint model may be easily customised to any MRI or CT geometry using free-form deformation. Three 'split line' patterns (medial–lateral, anterior–posterior and random) were implemented in a finite element model with constitutive properties referring to this 'split line' orientation as a finite element fibre field. The medial–lateral orientation was similar to anatomy and was derived from imaging studies. Model predictions showed that 'split lines' are formed along the line of maximum principal strains and may have a biomechanical role of protecting the cartilage by limiting the cartilage deformation to the area of higher cartilage thickness.

Keywords Cartilage fibre orientation · Finite element analysis · Cartilage stress distribution · Split lines

✉ Vickie B. Shim
  v.shim@auckland.ac.nz

[1] Auckland Bioengineering Institute, The University of Auckland, Auckland, New Zealand

[2] Centre for Musculoskeletal Research, Griffith Health Institute, School of Allied Health Sciences, Griffith University, Gold Coast, QLD, Australia

[3] Department of Engineering Science, The University of Auckland, Auckland, New Zealand

[4] School of Sport Science, Exercise and Health, University of Western Australia, Nedlands, WA, Australia

1 Introduction

Osteoarthritis (OA) causes the most widespread physical morbidity and impaired quality of life in the western world (Abramson et al. 2006; Wieland et al. 2005). Almost half of all people over the age of 60 and virtually all over the age of 80 will have osteoarthritis, costing billion dollars per year in all major developed countries (Arthritis New Zealand 2010). Yet the pathogenesis of cartilage degeneration is largely unknown, and the disease untreatable with no available drugs that can slow down the disease progression (Wieland et al. 2005). The situation is particularly alarming for the knee joint, which is the most complex joint in the body that also experiences the most injury. Even daily activities like normal walking subject it to forces up to six times body weight (Accident Compensation Corporation 2003), and this does not account for highly dynamic tasks such as stair climbing that constitute our daily loading stimulus. Moreover, participation in sports and recreational activities, encouraged for all age groups, is 'wreaking havoc with knees worldwide' (Foy 2001) to the point of being described as 'an epidemic' (Accident Compensation Corporation 2003; Bollen and Scott 1996). Much of the damage is to cartilage, a mechanosensitive tissue maintained by a single cell type—the chondrocyte. Although cartilage has a very thin layer, it deforms during movement altering the contact surface area and magnitude of stress within the tissue (Wang et al. 2001). Consequently, cartilage damage due to knee injuries reduces tissue integrity and alters stress levels significantly.

The key feature in articular cartilage that is known to affect mechanical response is its unique layered microarchitecture with characteristic collagen fibre orientation (Aspden et al. 1981). In the deep zone of the tissue, the collagen fibres are aligned perpendicular to the joint surface, while the superficial layers of the tissue exhibit collagen fibre orientations

tangential to the joint surface. The planar orientation of collagen fibres in the superficial layer also shows specific patterns called 'split lines'. It has been postulated that 'split lines' are aligned according to principal stress directions that cartilage experiences during joint movement (Below et al. 2002). Some researchers used biomechanical experiment to analyse the role of 'split lines' in the articular surface. Mizrahi et al. (1986) measured the in-plane deformation of the articular surface and found that the deformation was the least along the 'split line' direction. Kamalanathan and Broom (1993) also performed biomechanical experiment and concluded that 'split lines' in the surface of articular cartilage may provide protection from the influence of distending forces. Other investigators have used computational methods to analyse the effects of fibre orientation on cartilage mainly using finite element (FE) analysis. These studies demonstrated that microarchitecture, especially the depth-dependent collagen orientation and 'split line' patterns, plays an important role in cartilage stress redistribution (Li et al. 2009; Mononen et al. 2011) as well as deformation. In fact, FE models have been widely used in investigating stress or contact pressure in the tibiofemoral or patellofemoral cartilage (Besier et al. 2005; Donahue et al. 2002; Henak et al. 2013; Pena et al. 2006; Yang et al. 2010). However, it is still not clear what the biomechanical roles of 'split lines' in the articular surface are. In particular, the influence of collagen fibre orientation and 'split line' patterns on stress distribution during daily activities such as walking has not been investigated. Therefore, the aim of this study is to use a subject-specific FE model of the knee joint to investigate the biomechanical role of collagen fibre orientation, especially on the articular surface (i.e. split lines). The present study is focussed on how 'split lines' influence internal stress and strain distribution patterns in the tibiofemoral cartilage during the stance phase of gait. Our hypothesis is that 'split lines' play a role in shifting the pattern of cartilage deformation towards regions of thicker cartilage.

2 Methods

2.1 Overall modelling framework

The modelling framework is composed of two levels—joint and tissue levels (see Fig. 1). The joint-level model is a whole joint knee FE model consisting of the femur, tibia, meniscus and all four ligaments. Cartilage layers at the tibiofemoral articulation were chosen as the outer layers of bone using the numerical integration points, called Gauss points. The efficiency of this approach to assigning cartilage has been validated in previous work (Shim et al. 2015). The loads experienced by the knee during gait were simulated with this whole joint knee model. This model was linked with detailed

models of cartilage and meniscus that contain accurate fibre orientations. Strain values at Gauss points located at the bone–cartilage interface were used as displacement boundary condition for the tissue-level model. This way the tissue-level stress and strain in cartilage during gait was analysed in an accurate and efficient manner.

The macroscale FE model of the knee was generated from Visible Human images (NLM, Bethesda, MD) using a previously developed technique (Shim et al. 2007) which uses high-order cubic Hermite interpolation functions and an optimisation-based geometric fitting procedure (Fernandez et al. 2004) to generate meshes with C1 continuous smooth surfaces. Our knee model is made up of three bones (femur, tibia, fibula), four ligaments, namely, anterior cruciate ligament (ACL), posterior cruciate ligament (PCL), medial collateral ligament (MCL) and lateral collateral ligament (LCL), and the menisci (Fig. 2). In the macroscale model, the cartilage layer was modelled using a Gauss point material assignment scheme (Shim et al. 2008) (Fig. 2d) . Firstly, cartilage regions in the tibiofemoral articulation were identified from the Visible Human images, and the Gauss points that were in the cartilage regions were identified and assigned with cartilage material properties. Therefore, our model had four different tissues materials with their corresponding constitutive properties. For bones, cortical (Anderson et al. 2005) and cancellous (Dalstra et al. 1993) and subchondral regions were modelled as linear elastic material with representative modulus and Poisson's ratio values obtained from the literature (Anderson et al. 2005; Dalstra et al. 1993). Cartilage and meniscus were modelled as single phase, linear elastic and isotropic materials. Modulus and Poisson's ratio values used in linear elastic materials are summarised in Table 1.

Ligaments were modelled as incompressible neo-Hookean materials with hyperelastic and isotropic material properties and used values reported in Pena et al. (2006) and shown in Table 2.

### 2.2 Creation of a subject-specific FE model with free-form deformation

The macroscale FE model was customised to a subject-specific model with the subject's MRI data (29 years old, female) using the free-form deformation (FFD) method (Fernandez et al. 2004). Firstly, the anatomical landmark points were identified from the generic knee mesh. Then corresponding target points were found from the patient's MRI scans. The differences between the landmark and target points were minimised to customise the generic mesh to a subject-specific mesh. Figure 3 illustrates this process.

Gait analysis was performed with the subject whose MRI was used in FFD customisation. Using a previously developed method (Oberhofer et al. 2009), we obtained kinematic and kinetic data. Specifically, an 8-camera VICON Work-
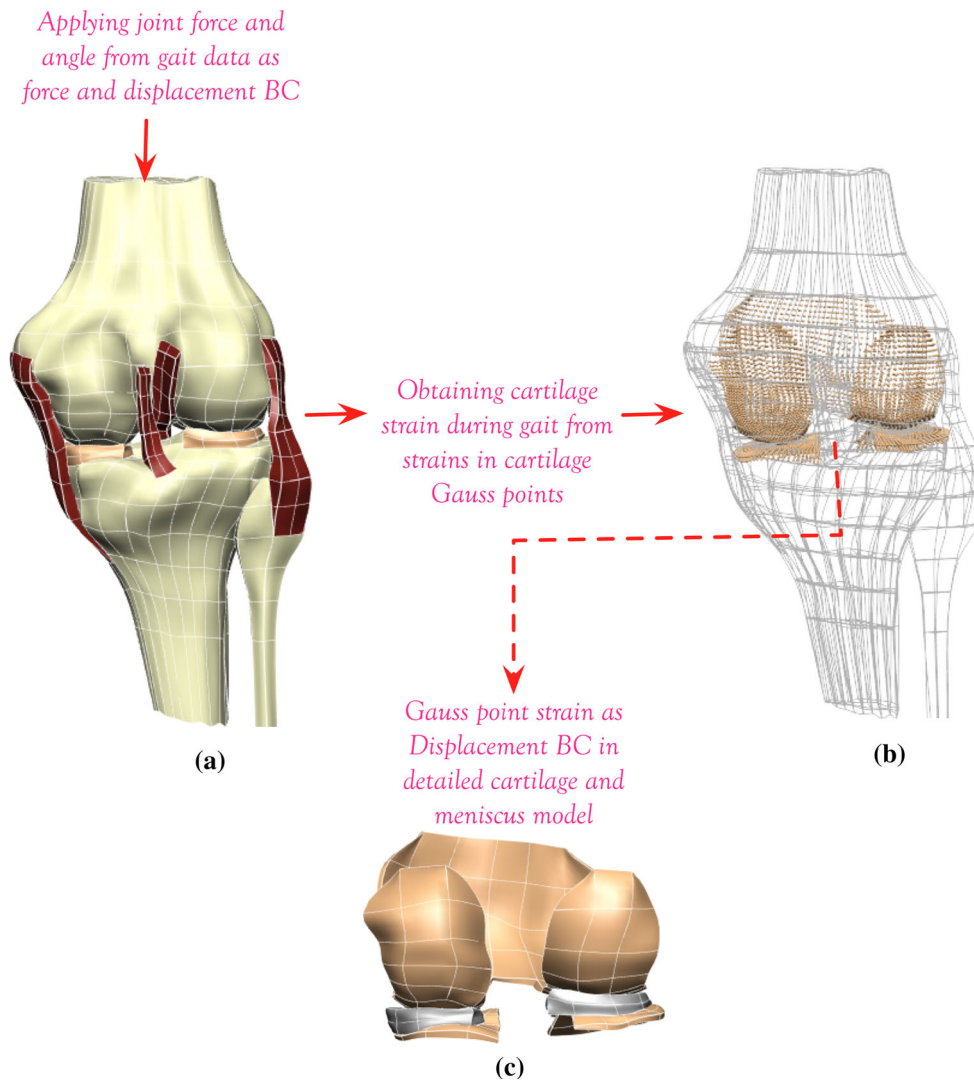
Fig. 1 Modelling pipeline consisting of whole joint cartilage strain from gait analysis passed to separate cartilage–menisci model as boundary conditions. **a** Whole knee model with major bones and soft tissues. **b** Inside view of the whole knee model showing Gauss points assigned with cartilage material properties. **c** Separate mesh generated detailed analysis of cartilage stress distribution

Visible Human Image stack

Initial Mesh

Final fitted Mesh

Locations of cartilage gauss points (grey)
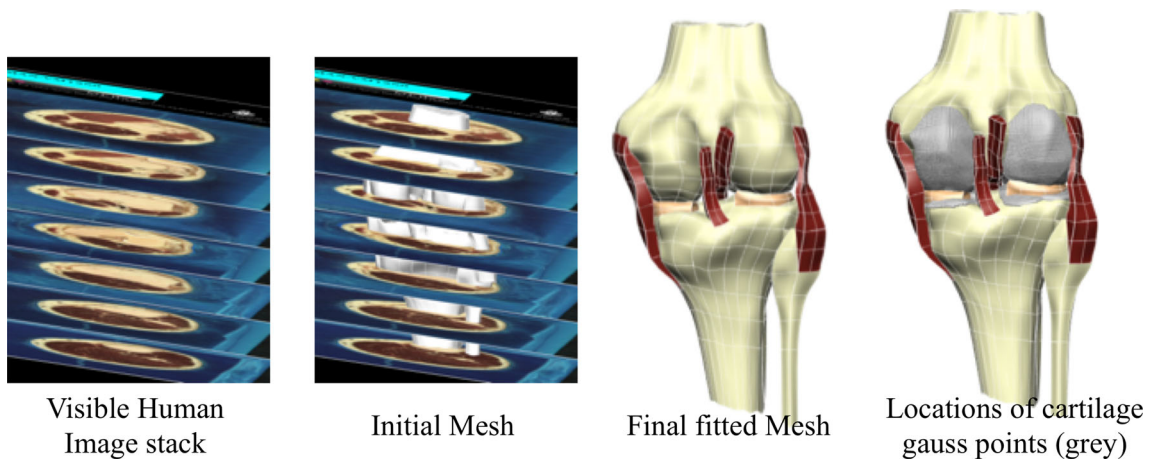
Fig. 2 Steps involved in the generation of the knee joint FE model. The cartilage layer is represented with Gauss points in this macrolevel model (shown on far *right*)

Table 1 Modulus and Poisson's ratios

	Modulus (MPa)	Poisson's ratio	References
Cortical bone	17,000	0.3	Shim et al. (2008)
Cancellous bone	650	0.3	Dalstra et al. (1993)
Cartilage	5	0.46	Li et al. (2001)
Menisci	59	0.49	LeRoux and Setton (2002)

Table 2 C_1 values for ligaments

	ACL	PCL	MCL	LCL
C_1 (MPa)	6.06	6.43	5.38	6.06

station version 5.0 (Oxford Metrics Ltd., Oxford, England) was used at 100 Hz. The Cleveland Clinic Marker set, which is routinely used in clinical gait analysis was adopted. The marker set consists of 15 skin markers on anatomical landmarks and an additional 12 markers on rigid plates wrapped around shank and thigh. Ground reaction forces were measured by two Bertec force plates (Bertec Corporation, OH, USA). Combining all kinematic data and ground reaction force data, an inverse dynamic analysis procedure was used to calculate the reactive forces and moments at all joints. The values for the knee joint were used as subject-specific boundary conditions for our FE analysis. Specifically, the whole system was solved quasi-statically for four key loading points in the stance phase of the gait cycle, namely heel strike, opposite toe-off, heel-rise and contralateral toe-off. First, flexion rotation, internal–external rotation and medial–lateral translation were applied to the mesh. And then the ground reaction force and moments were applied to solve for varus–valgus rotation, anterior–posterior translation and superior–inferior translation, which determines the knee contact mechanics. Contact between the bones and menisci was modelled as frictionless contact, while contact between the bone and ligaments was modelled as tied contact. Stress strain distribution at the tibiofemoral articulation were computed and passed on to the tissue level FE model of cartilage and meniscus, described below in Sect. 2.3.

2.3 Creating tissue-level FE model of cartilage and meniscus with anatomically based fibre orientation

The subject's MRI was used to identify the cartilage layer shapes and thickness on tibiofemoral articulation and separate meshes for femoral and tibial cartilage layers were created. Therefore the tissue-level FE model consisted of femoral and tibial cartilage layers and meniscus (Fig. 4).

The cartilage and meniscus layers were modelled as transversely isotropic biphasic materials. Since our boundary conditions are instantaneous points in the gait cycle (i.e.

heel strike and toe-off) and the instantaneous response of biphasic cartilage was shown to be equivalent to that of an incompressible material (Ateshian et al. 1994), a transversely isotropic incompressible elastic material formulation by Garcia et al. (1998) was adopted. They showed that the solution of a biphasic transversely isotropic problem at time zero is equivalent to that of an incompressible transversely isotropic elastic problem. Specifically, the elastic modulus of the equivalent incompressible material was found in terms of the elastic constants of the solid skeleton in the biphasic material from Eqs. 1 and 2,

$$E_{11} = \frac{E_{11}^{(s)}\left[1 - 4v_{31}^{(s)} + 2\left(1 - v_{12}^{(s)}\right)\left(E_{33}^{(s)}/E_{11}^{(s)}\right)\right]}{1 + \left(1 - v_{12}^{(s)2}\right)\left(E_{33}^{(s)}/E_{11}^{(s)}\right) - 2v_{31}^{(s)}\left(1 + v_{12}^{(s)}\right) - v_{31}^{(s)2}\left(E_{11}^{(s)}/E_{33}^{(s)}\right)}$$

(1)

$$E_{33} = \frac{E_{33}^{(s)}\left[1 - 4v_{31}^{(s)} + 2\left(1 - v_{12}^{(s)}\right)\left(E_{33}^{(s)}/E_{11}^{(s)}\right)\right]}{2\left(1 - v_{12}^{(s)}\right)\left(E_{11}^{(s)}/E_{33}^{(s)}\right) - 4v_{31}^{(s)2}}, \quad v_{12} = 1 - 0.5\left(\frac{E_{11}}{E_{33}}\right)$$

(2)

where $E^{(s)}$ denotes elastic constants of the solid skeleton of cartilage, while E denotes the equivalent incompressible elastic constants. The subscript denotes planes in the system with 1–2 being the plane of isotropy. In this study, the equivalent elastic incompressible properties were obtained from the solid skeleton properties of cartilage reported by Cohen et al. (1993), who obtained the values from cartilage indentation tests.

The cartilage and meniscus models were then fitted with an imaging-based fibre field representing the surface layer split line pattern taken from Below et al. (2002). Firstly, a reference material coordinate system (curvilinear and orthogonal) is defined based on the finite element coordinate system $(x_1 - x_2 - x_3)$. Secondly, a mutually orthogonal curvilinear material coordinate system $(u_1 - u_2 - u_3)$ for the deformable body is defined, which is used to represent the fibre vector direction and a further two arbitrary directions (orthogonal) to complete the structure-based 3D material coordinate system. For each point in the cartilage, three sequential rotations (Carden sequence) are then performed using the computed Euler angles to align the initial reference material coordinate system with the final structure-based material coordinate system. Following these rotations, direction one (x_1) aligns with the fibre vector direction (u_1). These Euler angles are then fitted as a finite element nodal field (i.e. nodally based infor-
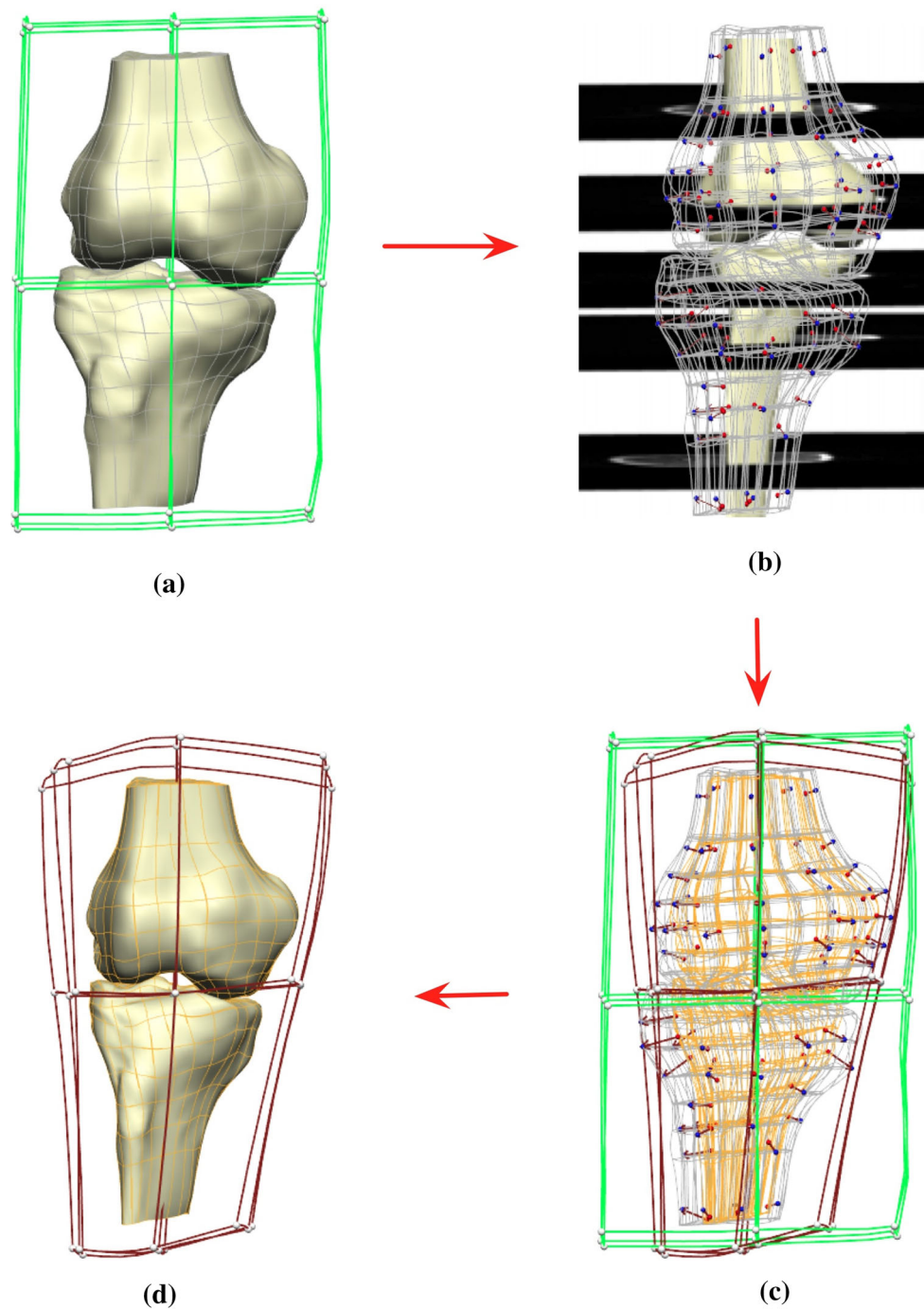
Fig. 3 Procedures for obtaining a subject-specific FE model of the knee with free-form deformation. **a** Generic mesh form visible human images along with the initial host mesh. **b** Getting target points for mesh morphing by aligning the generic mesh with subject's MRI. *Red points* are target points form MRI and *blue* are landmarks from the generic mesh. **c** Deforming the host mesh to minimise the distance between landmark and target points. *Green* is the initial host mesh and *purple* is deformed host. **d** Morphing the mesh according to the host mesh deformation pattern to get a subject-specific mesh

mation field) and aligned with the fibre orientation within the cartilage. For more details on determining Euler angles, the reader is referred to Mithraratne et al. (2010).

To analyse the influence of split lines on stress distribution, three different split line patterns were tested in a similar manner to Mononen et al. (2011); (1) normal split
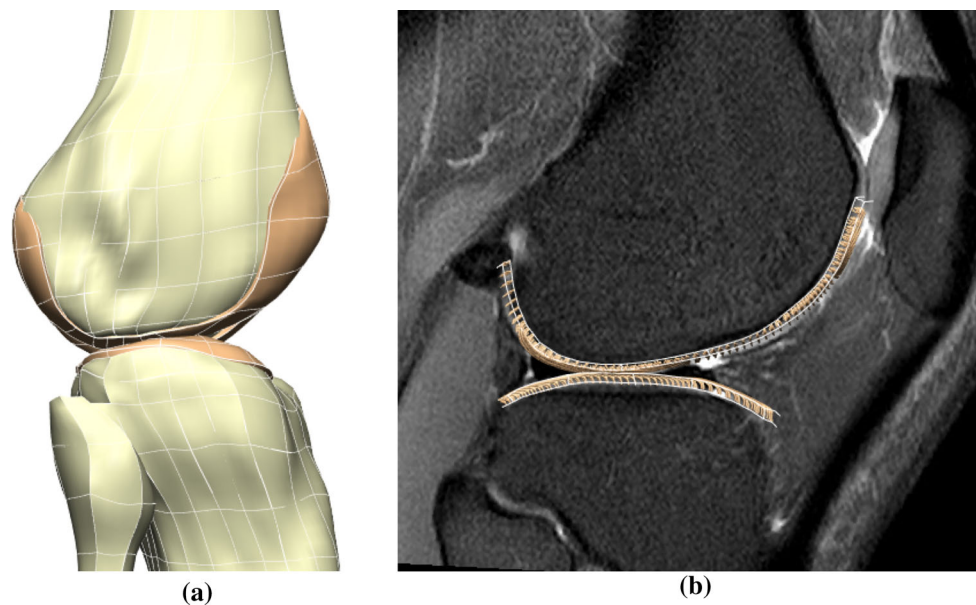
Fig. 4 Getting cartilage geometry and thickness from the MRI. **a** FE model with cartilage layer, **b** MRI scan with the FE model of cartilage layers. The collage fibre orientation embedded in the model is shown

line reflecting the actual pattern shown in Below and colleagues work (2002); (2) anterior–posterior (AP) line where tangential layer collagen fibres run in the AP direction; and (3) random fibre orientation (Fig. 4).

Once the depth-dependent fibre orientation and split lines patterns were implemented, the final models were solved with strain values obtained from the whole joint-level knee model. Nodes from the top layer of the femoral cartilage and the bottom layer of the tibial cartilage were constrained according to the strain values at the corresponding Gauss points. The contact between cartilage and meniscus were described using frictionless conditions. The role of split lines in the articular cartilage was investigated using the following three measurements computed from the FE analysis. First, von Mises stress patterns were used to show the overall stress distribution patterns. Maximum principal strain vectors were also used to identify the directional properties of split line patterns, particularly how it influences the development of tensile strain and its direction. Finally, the amount of in-plane cartilage deformation was measured by computing the total amount of deformation in the articular surface. This was done by comparing undeformed and deformed meshes of the femoral cartilage for all three cases of split line patterns tested. The total amount of deformation was calculated and compared the three split line patterns. Statistical significance of the differences was tested using paired two-sample t test. The models were solved using the open-source finite element software CMISS (www.cmiss. org), which has been developed as a part of the Physiome Project (Hunter and Borg 2003) and is freely available for academic use.

3 Results

The amount of deformation predicted by the FE model was compared with values reported in a previous study by Lui and colleagues, which measured cartilage deformation during stance phase of gait using fluoroscopy (Liu et al. 2010) (Fig. 5).

The work of Liu et al. is shown in blue (with error bars) and the results from this study are shown in red. The predicted cartilage deformation pattern followed the measured values reported by Liu et al. (2010) (Fig. 6). However, while the predicted medial values were close, the model predicted lateral side deformation was larger than that measured by Liu et al., but was within the standard deviation of their measurement, except at 100 % of gait. The predicted cartilage deformation was the largest during the opposite toe-off phase of gait.

Von Mises stress distribution patterns on the femoral cartilage were plotted for the three fibre orientation patterns tested (normal, AP and random split line patterns) (defined in Fig. 5). Figure 7 shows these surface von Mises stress patterns at heel strike, opposite toe-off, heel-rise and toe-off for the three fibre orientation patterns.
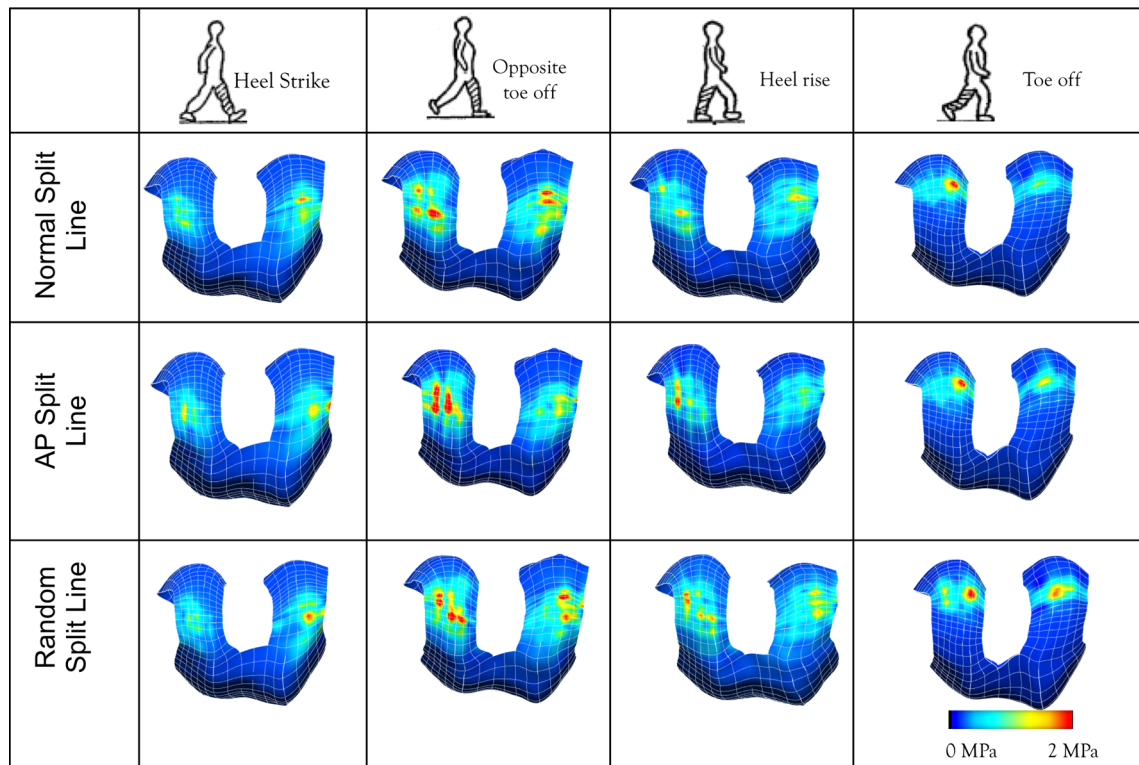
The von Mises cartilage stress distribution revealed that the pattern is highly dependent on the fibre orientation at the articular surface as well as the contact area. The contact area changed during the stance phase of gait, which is reflected in the peak stress pattern changes at different stages of the stance phase. When normal split line pattern was used, the peak stress value was 2.1 MPa and occurred during the opposite toe-off point of the gait cycle. When split line direction was changed from normal to AP and to
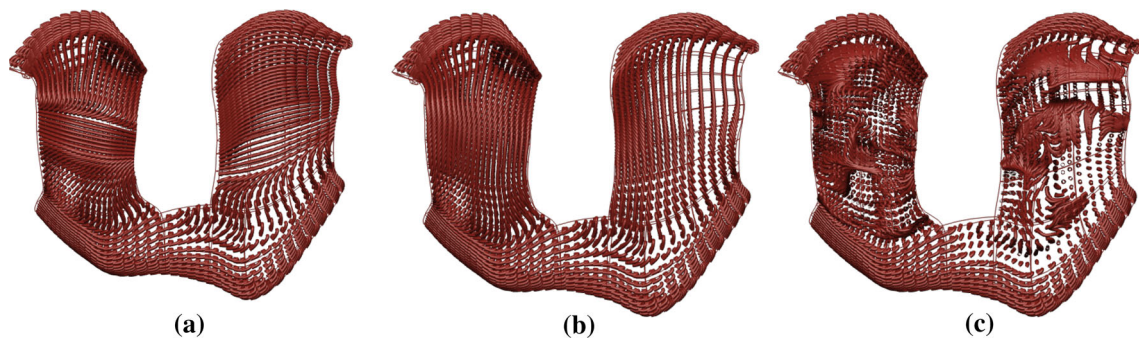
Fig. 5 Three split line patterns tested in our tissue level cartilage FE simulation. **a** Normal split line, **b** split line in AP direction only, **c** random split line
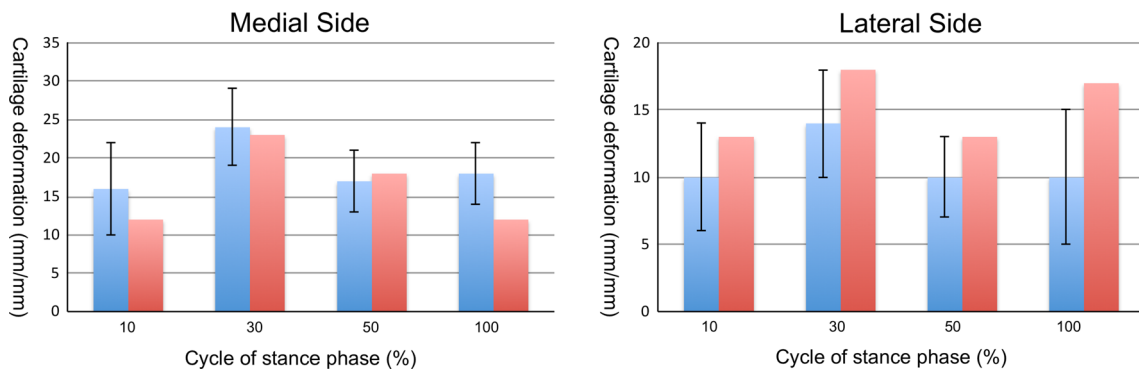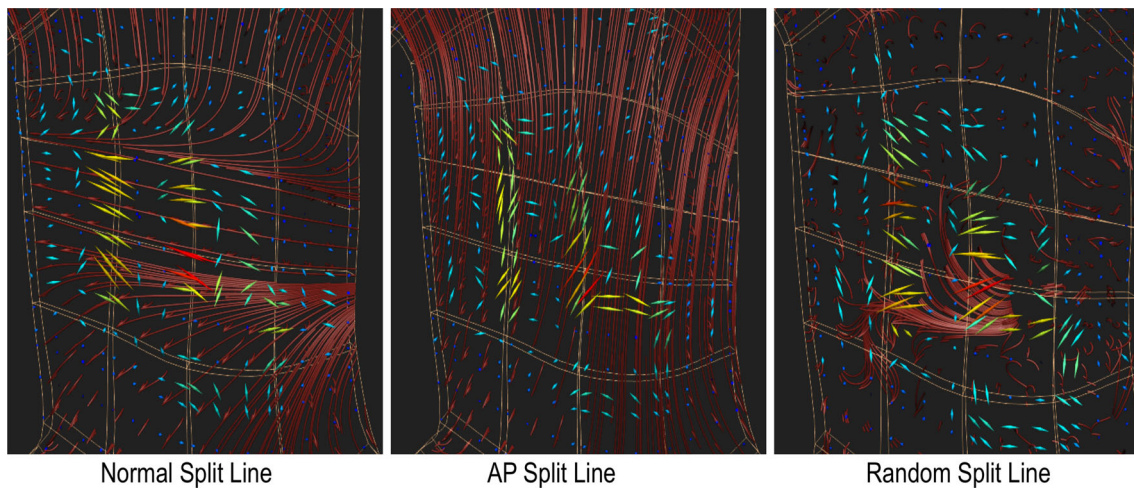

Fig. 6 Comparison between predicted and measured cartilage deformation on the medial and lateral tibial condyles. Liu et al. is shown in *blue* and the current study shown in *red*

Fig. 7 Von Mises stress distribution on the femoral cartilage during stance phase of the gait. *Left* is medial and *right* is lateral. *Red* is a peak of 2 MPa

Fig. 8 Vector plot of maximum principal strain in cartilage for (*left*) normal split line; (*middle*) anterior–posterior split line; and (*right*) random split line pattern

random, the peak stress value also increased slightly to 2.3 and 2.4 MPa, respectively. However, it was the stress distribution pattern that changed more drastically when the split line direction was changed. The influence of split line is most visible when the direction switched from a medial–lateral direction to anterior–posterior (first and second rows of Fig. 7) where the peak stress region changed to align with the fibre orientation. Specifically, examining the stress during opposite toe-off and heal rise, it is clear the peak von Mises 'hot spots' in the area of contact have shifted from a medial–lateral elongation to anterior–posterior elongation pattern. To highlight the influence that the split line pattern is having, a simulation with a random split line pattern generated peak stresses in random locations, indicating that the location of fibre split may cause peak stress to occur especially when this region coincides with the area of contact.

The strain vector plot showed that the direction of maximum principal strain aligned with the fibre orientation (Fig. 8). The change in fibre orientation changed the strain vector orientation accordingly when run using the same boundary conditions. This confirms that the split lines are formed along the principal strain direction as postulated by others (Below et al. 2002).

The in-plane deformation of the femoral cartilage was also dependent on fibre orientation. The amount of in-plane cartilage deformation was measured by computing the total deformation of femoral cartilage meshes for all three cases of split line tested (normal, AP and random). Model predictions showed that the cartilage model with random split lines had more cartilage deformation than the other cases and the difference was statistically significant ($p = 0.01$) (Fig. 9).
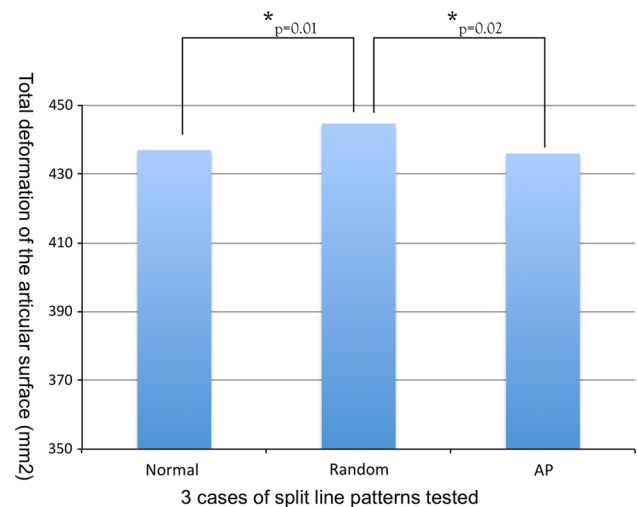
Fig. 9 Comparison of total in-plane deformation of the three split line patterns tested. The cartilage mesh with random split line pattern (*centre*) showed a significantly larger amount of total deformation than the other two cases

4 Discussion

This study presents a computational framework developed to analyse stress distribution patterns in the femoral cartilage during gait. We used a subject-specific finite element model that is composed of two levels; (1) a joint-level model that has all major bones, ligaments and meniscus of the knee. Cartilage layers were embedded inside the bone model as a set of Gauss point that occupies the area of cartilage layer in the knee; and (2) a cartilage and meniscus model that contains accurate collagen fibre distribution pattern including the 'split line' patterns in the superficial region of the cartilage.

The strength of this approach is that one can analyse cartilage mechanics with subject-specific loading conditions while retaining greater computational efficiency. In fact, it took about than two hours to run the whole joint model for one point in the gait cycle, but only a few minutes to run the cartilage model using a standard PC. The complexity of the whole knee model and the high computational cost were some of the reasons that previous FE models had cartilage layers run mainly with simplified loadings conditions (Gu and Li 2011; Mononen et al. 2011; Shirazi and Shirazi-Adl 2009). However, the current approach allowed investigation of various aspects of cartilage mechanics with a full FE model of the knee joint using physiological and subject-specific loading conditions.

The main focus of this study was to investigate the role of 'split line' patterns in stress distribution in the femoral cartilage. It has been postulated that 'split lines' are oriented according to joint movements and principal stress directions. The results showed that the presence of 'split lines' changed the stress distribution patterns, and the location and distribution of peak stresses followed the 'split line' patterns. The strain vector plots confirmed that the 'split lines' do get formed along the line of maximum principal strain. The analysis of in-plane cartilage deformation revealed an interesting biomechanical role of 'split lines', in that it limits the deformation of cartilage to the central region of cartilage, which coincides with the thickest cartilage zones. Therefore, this study suggests that the 'split lines' in the articular surface play a role in guiding the deformation pattern of cartilage and limiting it to the region with thicker cartilage.

There have been previous FE studies that investigated the role of 'split lines' in tibiofemoral cartilage (Gu and Li 2011; Mononen et al. 2011). These studies also showed that 'split lines' controlled stress and strain values. However, they used either FE models of the cartilage layer only or simplified knee joint models, and all used an axial loading to simulate their results. This study, in contrast, used a full knee joint FE model with boundary conditions from subject-specific gait data coupled to a tissue-level cartilage model. This way, the influence of 'split lines' on stress distribution within the cartilage was identified throughout the gait cycle. Furthermore, the role of split lines in keeping peak cartilage deformation to the central thicker region of cartilage during gait was also revealed. Split lines may be seen as providing an additional structural adaptation to loading that improves cartilage protection.

There are a few limitations that should be considered when interpreting the results in this study. The 'split line' pattern incorporated in this study was estimated from images of femoral cartilage in a previous anatomical study (Below et al. 2002), which had limited resolution. Therefore, the fibre orientation and location of fibre split pattern also had to be estimated from the images, which might have influenced the location of predicted peak stress. One might need to perform an anatomical dissection study to have better resolution images. However, a parametric study was performed to see the effect of 'split line' patterns by using three representative cases. In each case, the pattern of peak stress were heavily influenced by split line orientation and focussed towards the centre. Therefore, the findings from this study about the biomechanical role of 'split lines' are still valid despite the resolution of those images used in implementing fibre orientation. Secondly, we have not performed direct cadaveric validation of our model. Instead we have used a previous study by Liu et al. (2010) who reported measured cartilage deformation during stance phase of the gait. We found that our model prediction closely followed the measured pattern reported by Liu and colleagues. However, caution is required in interpreting this result as our predicted pattern deviates from that of Liu and colleagues especially at 100 % point of the stance phase of the gait cycle. One major reason behind this discrepancy can attributed to the difference between the subjects used in their and our study. Specifically, Liu and colleagues used a dataset of eight healthy subjects aged between 32 and 49 among whom six were males and two females. On the other hand, we used a gait data from a single female subject of 28 years old. The body mass index of the subjects from Liu et al. was $23.5 \, kg/m^2$, while our subject has the BMI of $21 \, kg/m^2$. Although our subject matches the qualitative description of 'healthy subjects' free from any knee abnormalities used in Liu et al., the details in body composition and age do not match perfectly. Due to these differences, our prediction does not completely match the measured deformation of Liu et al. However, the pattern matched relatively closely, and the amount of deviation at 100 % point of the stance phase was just above or below their standard deviation. Therefore, we are confident that our model is capable of recreating cartilage deformation patterns during gait. Finally, our knee joint models only have proximal parts of the femur and tibia, so we could not use muscle forces from gait analysis in our study. Muscle forces account for up to half the loading in a joint and should be considered future version of this work.

To conclude, we performed full subject-specific FE analysis of the knee joint to investigate the role of split lines in the tibiofemoral cartilage. We built a novel computational framework for investigating cartilage stress during gait. Our results showed that split lines are formed along the line of maximum strains, and it has a biomechanical role of protecting the cartilage by limiting the cartilage deformation to the area of higher cartilage thickness.

References

Abramson SB, Attur M, Yazici Y (2006) Prospects for disease modification in osteoarthritis. Nat Clin Pract Rheumatol 2:304–312

Accident Compensation Corporation (2003) The diagnosis and management of Soft tissue knee injuries: internal derangement. www.acc.co.nz/PRD_EXT_CSMP/groups/external.../wcmz003523.pdf

Anderson AE, Peters CL, Tuttle BD, Weiss JA (2005) Subject-specific finite element model of the pelvis: development, validation and sensitivity studies. J Biomech Eng 127:364–373

Arthritis New Zealand (2010) http://www.arthritis.org.nz/index.php/Osteoarthritis.html

Aspden RM, Hickey DS, Hukins DW (1981) Determination of collagen fibril orientation in the cartilage of vertebral end plate. Connect Tissue Res 9:83–87

Ateshian GA, Lai WM, Zhu WB, Mow VC (1994) An asymptotic solution for the contact of two biphasic cartilage layers. J Biomech 27:1347–1360

Below S, Arnoczky SP, Dodds J, Kooima C, Walter N (2002) The split-line pattern of the distal femur: a consideration in the orientation of autologous cartilage grafts. Arthroscopy 18:613–617

Besier TF, Gold GE, Beaupre GS, Delp SL (2005) A modeling framework to estimate patellofemoral joint cartilage stress in vivo. Med Sci Sports Exerc 37:1924–1930

Bollen SR, Scott BW (1996) Rupture of the anterior cruciate ligament—a quiet epidemic? Injury 27:407–409

Cohen B, Gardiner TR, Ateshian (1993) The influence of transverse isotropy on cartilage indentation behavior: a study of the human humeral head. Trans Orthop Res Soc 18:185

Dalstra M, Huiskes R, Odgaard A, van Erning L (1993) Mechanical and textural properties of pelvic trabecular bone. J Biomech 26:523–535

Donahue TL, Hull ML, Rashid MM, Jacobs CR (2002) A finite element model of the human knee joint for the study of tibio-femoral contact. J Biomech Eng 124:273–280

Fernandez JW, Mithraratne P, Thrupp SF, Tawhai MH, Hunter PJ (2004) Anatomically based geometric modelling of the musculo-skeletal system and other organs. Biomech Model Mechanobiol 2:139–155. doi:10.1007/s10237-003-0036-1

Foy MA (2001) Medicolegal reporting in orthopaedic trauma. Churchill Livingstone, Edinburgh

Garcia JJ, Altiero NJ, Haut RC (1998) An approach for the stress analysis of transversely isotropic biphasic cartilage under impact load. J Biomech Eng 120:608–613

Gu KB, Li LP (2011) A human knee joint model considering fluid pressure and fiber orientation in cartilages and menisci. Med Eng Phys 33:497–503. doi:10.1016/j.medengphy.2010.12.001

Henak CR, Anderson AE, Weiss JA (2013) Subject-specific analysis of joint contact mechanics: application to the study of osteoarthritis and surgical planning. J Biomech Eng 135:021003. doi:10.1115/1.4023386

Hunter PJ, Borg TK (2003) Integration from proteins to organs: the Physiome Project Nature reviews. Mol Cell Biol 4:237–243. doi:10.1038/nrm1054

Kamalanathan S, Broom ND (1993) The biomechanical ambiguity of the articular surface. J Anat 183(Pt 3):567–578

LeRoux MA, Setton LA (2002) Experimental and biphasic FEM determinations of the material properties and hydraulic permeability of the meniscus. J Biomech Eng 124:315–321

Li G, Lopez O, Rubash H (2001) Variability of a three-dimensional finite element model constructed using magnetic resonance images of a knee for joint contact stress analysis. J Biomech Eng 123:341–346

Li LP, Cheung JT, Herzog W (2009) Three-dimensional fibril-reinforced finite element model of articular cartilage. Med Biol Eng Comput 47:607–615. doi:10.1007/s11517-009-0469-5

Liu F, Kozanek M, Hosseini A, Van de Velde SK, Gill TJ, Rubash HE, Li G (2010) In vivo tibiofemoral cartilage deformation during the stance phase of gait. J Biomech 43:658–665. doi:10.1016/j.jbiomech.2009.10.028

Mithraratne K, Hung A, Sagar M, Hunter P (2010) An efficient heterogeneous continuum model to simulate active contraction of facial soft tissue structures. In: 6th World congress of biomechanics (WCB 2010). Springer, Singapore, pp 1024–1027, 1–6 August, 2010

Mizrahi J, Maroudas A, Lanir Y, Ziv I, Webber TJ (1986) The "instantaneous" deformation of cartilage: effects of collagen fiber orientation and osmotic stress. Biorheology 23:311–330

Mononen ME, Julkunen P, Toyras J, Jurvelin JS, Kiviranta I, Korhonen RK (2011) Alterations in structure and properties of collagen network of osteoarthritic and repaired cartilage modify knee joint stresses. Biomech Model Mechanobiol 10:357–369. doi:10.1007/s10237-010-0239-1

Oberhofer K, Mithraratne K, Stott N, Anderson I (2009) Anatomically-based musculoskeletal modeling: prediction and validation of muscle deformation during walking. Vis Comput 25:843–851. doi:10.1007/s00371-009-0314-8

Pena E, Calvo B, Martinez MA, Doblare M (2006) A three-dimensional finite element analysis of the combined behavior of ligaments and menisci in the healthy human knee joint. J Biomech 39:1686–1701. doi:10.1016/j.jbiomech.2005.04.030

Shim VB, Batteley M, Anderson IA, Munro JT (2015) Validation of an efficient method of assigning material properties in finite element analysis of pelvic bone. Comput Methods Biomech Biomed Eng 18(14):1495–1499

Shim VB, Pitto RP, Streicher RM, Hunter PJ, Anderson IA (2007) The use of sparse CT datasets for auto-generating accurate FE models of the femur and pelvis. J Biomech 40:26–35

Shim VB, Pitto RP, Streicher RM, Hunter PJ, Anderson IA (2008) Development and validation of patient-specific finite element models of the hemipelvis generated from a sparse CT data set. J Biomech Eng 130:051010. doi:10.1115/1.2960368

Shirazi R, Shirazi-Adl A (2009) Computational biomechanics of articular cartilage of human knee joint: effect of osteochondral defects. J Biomech 42:2458–2465. doi:10.1016/j.jbiomech.2009.07.022

Wang CC, Hung CT, Mow VC (2001) An analysis of the effects of depth-dependent aggregate modulus on articular cartilage stress-relaxation behavior in compression. J Biomech 34:75–84

Wieland HA, Michaelis M, Kirschbaum BJ, Rudolphi KA (2005) Osteoarthritis—an untreatable disease? Nat Rev Drug Discov 4:331–344

Yang NH, Nayeb-Hashemi H, Canavan PK, Vaziri A (2010) Effect of frontal plane tibiofemoral angle on the stress and strain at the knee cartilage during the stance phase of gait. J Orthop Res 28:1539–1547. doi:10.1002/jor.21174